# Shape of a cohesive granular heap

Alain de Ryck, Rodrigo Condotta, John A. Dodds

# Shape of a cohesive granular heap

Alain de Ryck*, Rodrigo Condotta, John A. Dodds

*École des Mines d'Albi-Carmaux, UMR 2392 du CNRS, route de Teillet, 81000 Albi, France*

**Abstract**

We propose an analytical expression for the shape of a heap of cohesive powder when the cohesion is constant, and when the cohesion increases proportionally with the stresses applied. From the results obtained, we discuss the possibility to extract quantitative information on the flowability of a powder from this shape.

*Keywords:* Cohesion; Particle technology

## 1. Introduction

When a non-cohesive granular media (like dry sand) is poured from a single point, it forms a conical pile. The angle of the free surface from the horizontal $\phi$ is called the angle of repose (Fig. 1-a). The explanation, given by Coulomb, is that granular media sustain shear stresses as in solid friction. The pile remains stable if in all parts we have $\tau < \mu\sigma$, where $\tau$ and $\sigma$ are, respectively, the shear and normal stress; $\mu$ is called the apparent coefficient of friction of the granular media.

This solid friction behaviour limits the slope of a granular pile to a maximum value given by $\mu$. This maximum slope is obtained by the pouring experiment described above, leading to a simple experimental measurement of the apparent coefficient of friction: $\mu = \tan\phi$.

This description remains valid whilst the inter-particles forces are negligible compared to gravity. When these forces are of same order of magnitude or greater than the weight of the particles, the powder is said cohesive and the stability criterion becomes:

$$\tau < \mu\sigma + c, \tag{1}$$

where $c$ is the so-called cohesion.

When cohesion is present, which is the case for fine particles (their size $d$ is less than a ten micron), or when there is some liquid meniscii between them (like wet sand), it is possible to build vertical slopes (Fig. 1-b). But the elevation $L$ is limited in size. Coulomb's method of wedges [1] leads to:

$$L < \frac{4\cos\phi}{1-\sin\phi}\lambda \tag{2}$$

where $\lambda = c/\rho g$ is a length obtained by the ratio between inter-particles forces per unit area $c$ and gravitational forces per unit volume $\rho g$.

We apply this Coulomb's method of wedges in order to obtain an analytical expression for the profile of a 2-dimensional pile, in the case of constant cohesion (Section 2). We then discuss the possibility of measuring the friction coefficient $\mu$ and cohesion $c$ from a pouring experiment (Section 3). Finally, these results are compared to experiments (Section 4).

## 2. 2D semi-symmetric model

We focus our attention to the case of a semi-symmetric pile, whose height at a distance $x$ from the centre is $h(x)$. In order to be stable, the powder above the plane inclined by an

* Corresponding author.
*E-mail address:* deryck@enstimac.fr (A. de Ryck).

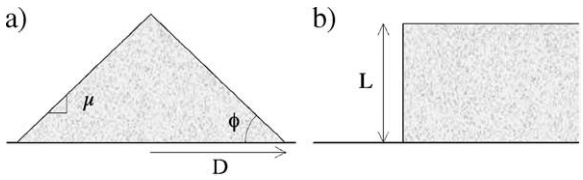


Fig. 1. a) Non-cohesive heap of radius $D$ at the base. The slope gives the coefficient of friction $\mu = \tan\phi$. b) Vertical elevation $L$ for a cohesive powder bed.

angle $\alpha$ must not slip (see Fig. 2) for $\alpha$ ranging from 0 to $\arctan(-h'(x))$. Its weight is given by:

$$P = \rho g \int_0^x (h(u) - h(x) + \tan\alpha(u-x))du. \quad (3)$$

The shear and normal stresses $\tau$ and $\sigma$ in the stability condition (Eq. (1)) are the ones exerted by the weight $P$ on the plane. They are given by:

$$\tau = \frac{P}{x}\sin\alpha\cos\alpha \quad \text{and} \quad \sigma = \frac{P}{x}\cos^2\alpha. \quad (4)$$

These expressions may be rewritten, using Eq. (3) and the trigonometric relations on double angle as:

$$\tau = \frac{1}{2}\rho g\left(z\sin 2\alpha - \frac{x}{2} + \frac{x}{2}\cos 2\alpha\right) \quad (5)$$

and

$$\alpha = \frac{1}{2}\rho g\left(z + z\cos 2\alpha - \frac{x}{2}\sin 2\alpha\right), \quad (6)$$

where

$$z = \frac{1}{x}\int_0^x (h(u) - h(x))du. \quad (7)$$

Eqs. (5) and (6) are the parametric equations for a circle in the $\tau-\sigma$ plane of radius $R = \rho g\sqrt{(x/2)^2 + z^2}/2$, centred on the point C ($\rho gz/2$, $-\rho gx/4$), passing through the origin (0,0) for $\tan\alpha = 2z/x$, and through the point S ($\rho gz$,0) for $\alpha = 0$ (Fig. 3).

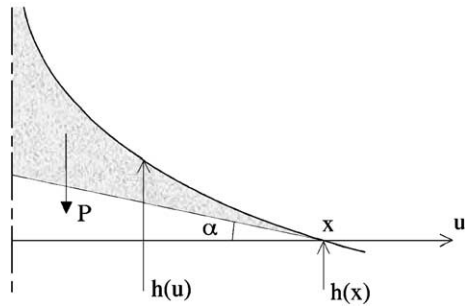


Fig. 2. Sketch of the heap profile. $P$ is the weight above the plane tilted by $\alpha$ from the horizontal and joining the free surface at the distance $x$ from the centre. $h(u)$ is the height of the heap at a position $u$ from the centre.

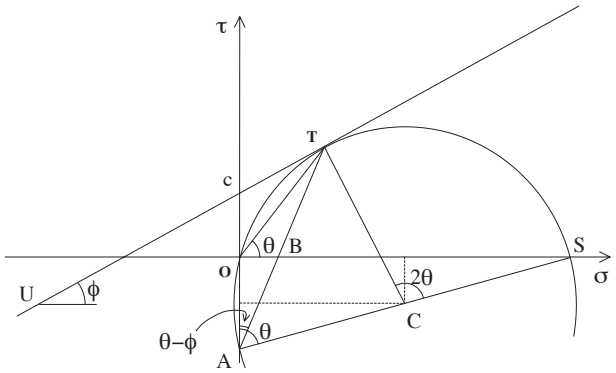


Fig. 3. Mohr circle in the shear-normal stress plane describing the shear ($\tau$) and normal stress ($\sigma$) acting on the plane when changing the tilting angle $\alpha$. In this figure, the Mohr circle tangents the Mohr–Coulomb failure criterion (Eq. (1)).

The limit of stability is then given when this Mohr-circle tangents the Coulomb criterion given by Eq. (1). It may be expressed, using the right-angled triangle UTC (Fig. 2), by:

$$\sin\phi = \frac{R}{\frac{c + \rho gx/4}{\tan\phi} + \rho gz/2}, \quad (8)$$

leading to:

$$z^2 - 2\mu\left(2\lambda + \frac{x}{2}\right)z + \left(1+\mu^2\right)\frac{x^2}{4} - \left(2\lambda + \frac{x}{2}\right)^2 = 0, \quad (9)$$

using the relation $\cos\phi = 1/\sqrt{1+\mu^2}$. If all the lengths are scaled by $\lambda$:

$$X = x/\lambda, Z = z/\lambda, \; H = h/\lambda, \quad (10)$$

Eq. (9) reduces to:

$$Z = \mu(2 + X/2) \pm 2\sqrt{(1+\mu^2)(1+X/2)}. \quad (11)$$

To solve this differential equation, it is convenient to notice that we have by derivation of Eq. (7):

$$(XZ)' = -XH'. \quad (12)$$

Then, introducing Eq. (11) in Eq. (12) leads to the slope of the heap profile as a function of the distance to the centre:

$$H' = -\mu(1 + 2/X) - \sqrt{\frac{1+\mu^2}{1+X/2}}(3 + 4/X). \quad (13)$$

The lower root of Eq. (11) is disregarded since it leads to a positive slope for the profile. Finally, Eq. (13) may be integrated in order to obtain the heap profile:

$$H = -\mu X - 2\mu\ln X - 4\sqrt{1+\mu^2} \times 3\sqrt{1+X/2} - \ln\frac{1+\sqrt{1+X/2}}{1-\sqrt{1+X/2}}\Bigg). \quad (14)$$

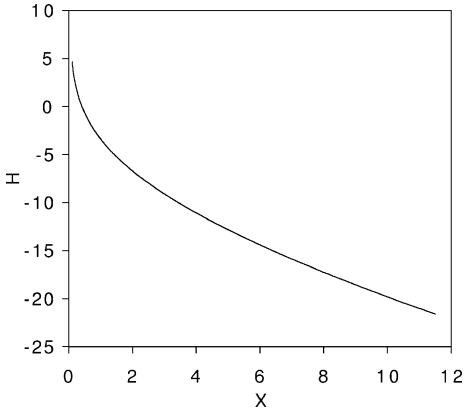


Fig. 4. Dimensionless shape of a cohesive heap for $\mu = 0.4$. The height and width are scaled by the cohesive length $\lambda$.

This profile diverges when $X \to 0$ and tends to have the slope $\mu$ when $X \to \infty$, as shown in Fig. 4.

### 2.1. Determination of the failure plane

The plane of incipient failure has an angle of inclination $\theta$, which is half the angle $\overline{TCS}$ (Fig. 3). As a consequence, we have $\overline{TOS} = \overline{TAS} = \theta$. From the first angle relation, it can be deduced the co-ordinates of the point of contact $T\left(\frac{c}{s-\mu}, \frac{cs}{s-\mu}\right)$, where $s = \tan\theta$ is the slope of the failure plane. Then, the co-ordinates of the point B are $\left(\frac{\rho g x/2}{s+(s-\mu)X/2}, 0\right)$. From the second angle relation, it can be deduced that $\overline{OAB} = \theta - \phi$. It leads to the relation:

$$\tan(\theta - \phi) = \frac{1}{s + (s-\mu)X/2}. \tag{15}$$

This equation can be easily solved to find the dependency of the slope of the failure plane versus its position $X$:

$$s = \mu + \sqrt{\frac{1+\mu^2}{1+X/2}}, \tag{16}$$

which means that the angle of failure has the limit $\theta \to \pi/4 + \phi/2$ when $X \to 0$, and the limit $\theta \to \phi$ when $X \to \infty$. The comparison between Eq. (13) and (16) shows that the failure plane is inside the powder bulk and does not tangent the free surface of the pile.

## 3. Discussion

### 3.1. Singularity at the origin

The theoretical result at the origin is a logarithmic divergence of the height of the pile. In practical situations, we have to stop the profile at a position $x$ which corresponds to the size $d$ of the particles or to the size of the particles distributor. An other size limitation is that the thin column of particles at the apex must sustain horizontal stresses due to air fluxes and impact of the flowing particles. To do that, the elevation of the mass centre $Z$ must not exceed the base $X$ by a factor corresponding to the ratio of horizontal to vertical stresses. In practise, we have to cut the profile at a distance $X_\beta$ for which we have:

$$Z/X = \beta\mu/2 \tag{17}$$

corresponding to a relative centre mass elevation $\beta$ times higher than the one obtained at infinity ($X \to \infty$). Fig. 5-a presents this dimensionless distance $X_\beta$ as a function of $\phi$ for $\beta = 5$ and $\beta = 10$. Fig. 5-b gives the corresponding angle $\Psi_\beta$ at this point.

One conclusion on the fact that the height at the origin is linked to the particle size or to the geometry of the distributor or to its equilibrium to horizontal forces disturbances is that it is then meaningless to measure a mean slope from the apex to the edge of the pile. This is not the case if we measure the local slope at the edge of the pile, as demonstrated in the next paragraph.

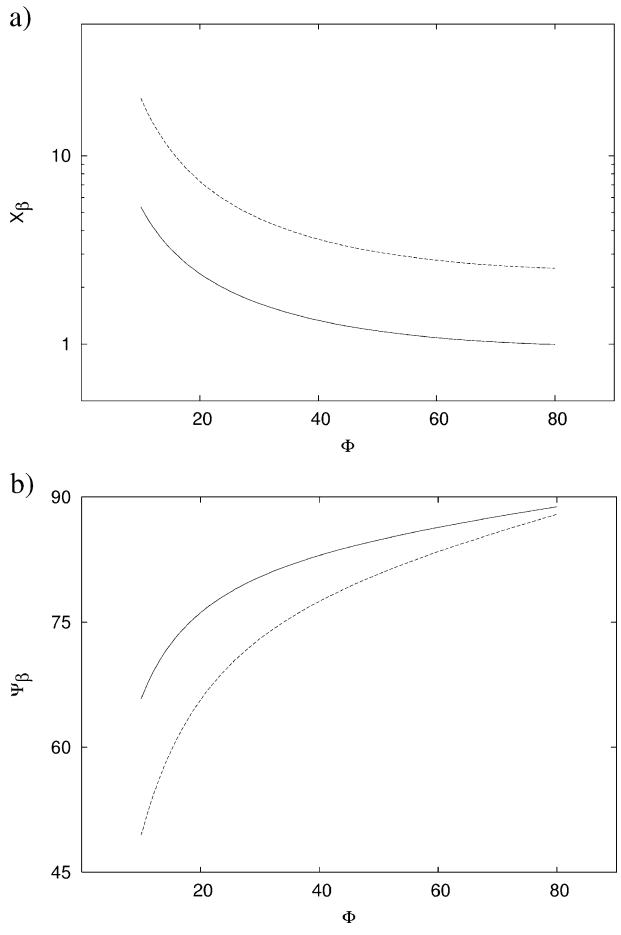


Fig. 5. Dimensionless distance of the base (a) and slope angle at the base (b) for $\beta = 5$ (continuous line) and $\beta = 10$ (dashed line).

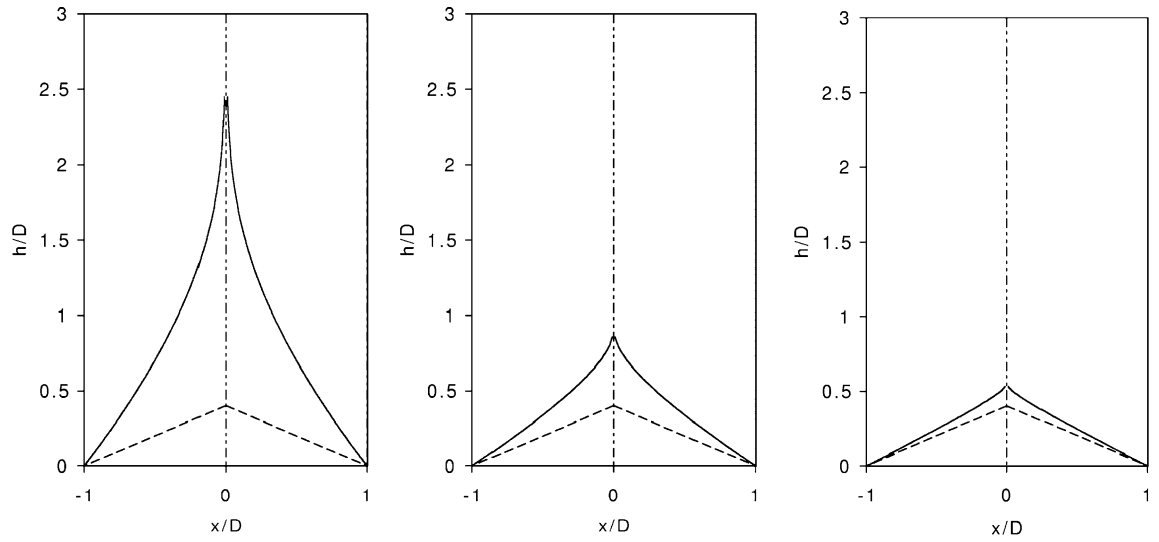


Fig. 6. Dimensionless shape of a cohesive heap. The height and width are scaled by the base radius $D$. a) $D=10\ \lambda$; b) $D=100\ \lambda$; c) $D=1000\ \lambda$.

### 3.2. Shape of the pile

Depending on the ratio between the length of the base of the pile $D$ and the cohesive length $\lambda$, we obtain different shapes of piles. As an example, the Fig. 6, from left to right, show respectively a ratio 1 to 10, 1 to 100 and 1 to 1000 between $\lambda$ and $D$, for the same coefficient of friction $\mu=0.4$. (For this figure, the divergence of the profile has been stopped at the grain size $x=d$, with $d=0.01\ D$.) When $\lambda$ is lower than three order of magnitude than the size of the pile, the latter has a shape which becomes close to the shape of a non-cohesive powder.

The slope $\psi$ at the base may be calculated from Eq. (13), as a function of the angle of internal friction and reduced position $X$ (Fig. 7). From that figure, we observe that it is feasible to obtain the cohesive length $\lambda$ from the measurements of both the angles $\psi$ and $\phi$.

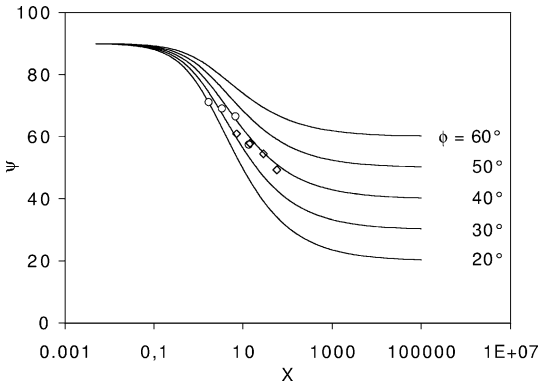


Fig. 7. Slope angle $\psi$ versus the scaled distance to centre $X=x/\lambda$, for 5 values of the friction angle $\phi$. Circles: slope angles from Fig. 10-a for the fine dolomite. The $x$ position is scaled with $\lambda=0.7$ mm to fit the $\phi$ values of Table 1. Squares: slope angles from Fig. 10-b for the mixed dolomite. The $x$ position is scaled with $\lambda=3$ mm to fit the $\phi$ values of Table 1.

### 3.3. Shape when cohesion is proportional to consolidation

For numerous cohesive powders, the yield criterion cannot be reduced to Eq. (1), with a constant cohesion [2]. It depends on the state of consolidation, and a better approximation is drawn on Fig. 8. In this model, the yield criterion, for a given consolidation $\sigma_c$ is a segment (of slope $\mu$) which ends at the point of co-ordinates ($\sigma_c$, tan $\delta\sigma_c$). The $\delta$ is found experimentally to be independent on the consolidation and called the internal coefficient of friction.

If we consider a pile of cohesive powder consolidated by its own weight, then the point T on Fig. 3 remains on the same line passing through the origin, of angle $\theta=\delta$. In that case, Eqs. (16) and (11) lead to the conclusion that $z/x$ is constant, then using Eq. (12) that the slope of the pile $-h(x)$ is constant. This slope may be determined by using the tangent relation in the OSA square triangle in Fig. 3. We

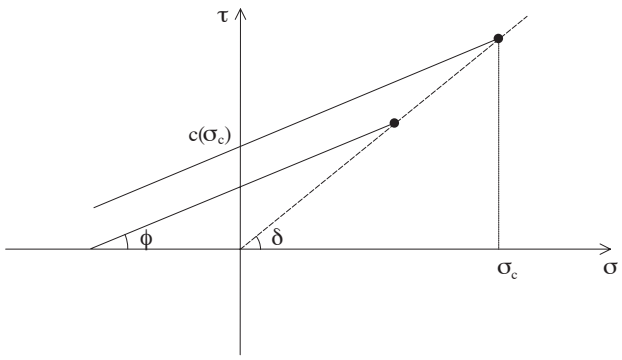


Fig. 8. Yield locii for a powder whose cohesion is proportional with the consolidation.

have:

$$\tan(2\delta - \phi) = 2z/x = -h'(x). \quad (18)$$

With such a powder, the heap formed is conical, with a slope $\psi = 2\delta - \phi$. From both the angles $\psi$ and $\phi$, we can obtain the cohesion:

$$c/\sigma_c = \tan((\phi + \psi)/2) - \tan\phi. \quad (19)$$

## 4. Experimental observations

### 4.1. Powders

In order to check the validity of such measurements, we have taken photographs of heaps of fine (F) and mixed (M) dolomites. These powders have been previously characterised for a European project [3]. Their volume weighted mean diameter $d_{4,3}$ is respectively 12.5 and 204 $\mu$m. There yield loci have been measured in a Jenike shear cell for 4 different normal stresses of consolidation $\sigma_c$ (Fig. 9) using the ASTM procedure [4]. The Table 1 gives for each yield locus the normal stress of consolidation $\sigma_c$, the values $\mu$ and $c$, which have been obtained by a linear fit. The last column of this table gives the ratio $c/\sigma_c$. Whether $c$ and $c/\sigma_c$ vary with the consolidation, which means that the real behaviour of these powders is in between the two descriptions proposed.

### 4.2. Results

These powders have been poured on a disk of radius $b = 4$ cm (Fig. 10-a,b) using the pluvation technique: the powder passes through two sieves of 250 and 315 µm, respectively, of same diameter than the disk which receives the powder.

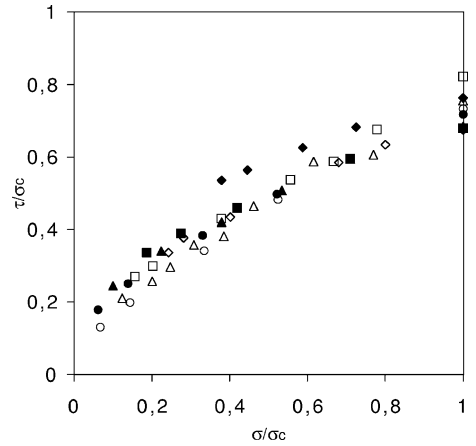


Fig. 9. Experimental yield locii for the dolomite powders, scaled by the consolidation normal stress $\sigma_c$. Black symbols: fine dolomite (diamonds, square, triangles and circles: respectively $\sigma_c = 3.66$, 6.58, 9.50 and 15.34 kPa). White symbols: mixed dolomite (diamonds, square, triangles and circles: respectively $\sigma_c = 2.11$, 5.03, 9.41 and 15.25 kPa).

Table 1
Measured parameters for the dolomites powders

| | $\sigma_c$ (kPa) | $\phi$ (°) | $c$ (kPa) | $\delta$ (°) | $2\delta - \phi$ (°) | $c/\sigma_c$ |
|---|---|---|---|---|---|---|
| Dolomite M | 3.66 | 24.7 | 0.90 | 35.2 | 45.7 | 0.25 |
| | 6.58 | 33.0 | 1.13 | 39.4 | 45.8 | 0.17 |
| | 9.50 | 32.2 | 1.41 | 37.9 | 43.6 | 0.15 |
| | 15.3 | 32.7 | 1.71 | 36.9 | 41.1 | 0.11 |

The slope angles $\psi(x)$ measured on the Fig. 10 have been compared with the slopes on the graph presented in Fig. 7, which compiles the results for a constant cohesion. The $X$ position is adjusted with a fit on the cohesive length $\lambda$ in order to match as close as possible the $\phi$ values of Table 1. This leads to $\lambda = 3 \pm 1$ mm for the fine dolomite and to $\lambda = 0.7 \pm 0.1$ mm for the mixed dolomite powder.

Nevertheless, it can be observed than close to the centre, we do not observe the high angles predicted. This discrepancy for $x \to 0$ seems due to the fact that the kinetic energy of the particles flowing down from the sieves is sufficient to break the mechanical equilibrium of the thin column of particles at the apex since it occurs for $X$ values close to 1 as expected by the curves given in Fig. 6-a.

Another explanation for this discrepancy close to the center ($x \to 0$) is that the cohesion is not constant since the yield locii (Fig. 9) are close to the model described by Fig. 8. In that case, we must observe a constant slope. If we extract a mean slope from the Fig. 10, we obtain $\psi = 68°$ for

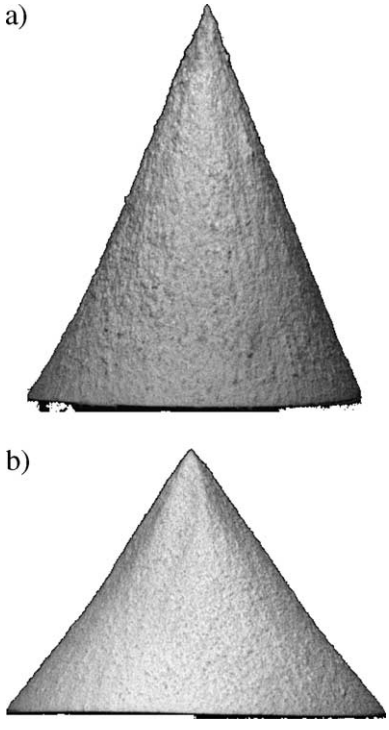


Fig. 10. Shape of heaps obtained by pluvation for the fine dolomite (a) and mixed dolomite (b).

the fine dolomite and $\psi = 56°$ for the mixed dolomite. These values are greater than that predicted by the theory $(2\delta - \phi)$ since, from Table 1, we expect respectively 47° and 44°. Disregarding this discrepancy, we can compute from Eq. (18) the ratio $c/\sigma_c = 0.54$ for the fine dolomite and $c/\sigma_c = 0.29$ for the mixed dolomite in order to estimate the cohesion of these powders and compare this estimation with the previous one.

### 4.3. Comparison with shear cell measurements

These results have been compared to the flow function $f_c = F(\sigma_1)$ obtained for the two powders and presented on Fig. 11 (respectively white diamonds and circles for the fine and mixed dolomites). To do this, we have to estimate the major principal stress $\sigma_1$ and the unconfined yield stress $f_c$. This comparison has been made using the two approximations studied: constant cohesion and cohesion proportional to the consolidation.

*Constant cohesion*—in the case of constant cohesion, $f_c$ is given by:

$$f_c = \rho g \lambda \frac{2\cos\phi}{1 - \sin\phi}, \tag{20}$$

and the maximum principal stress $\sigma_1$ depends on the height $z(\sigma_1 \approx \rho g z)$. It ranges from 0 at the centre to a value obtained with $z$ given by Eq. (11) with $X = D/\lambda$. The values obtained (black points in Fig. 11) are compared with the flow functions. The data obtained well extrapolate well the flow function for very low values of consolidation stresses.

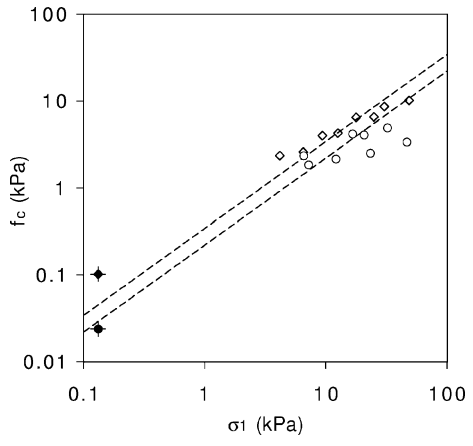


Fig. 11. Unconfined yield stress $f_c$ versus the maximum principal stress $\sigma_1$. White diamonds: flow function for the fine dolomite obtained from Fig. 9. White circles: flow function for the mixed dolomite obtained from Fig. 9. Black diamond: unconfined yield stress estimated from the shape of a fine dolomite heap with the hypothesis of constant cohesion. Black circle: unconfined yield stress estimated from the shape of a mixed dolomite heap with the hypothesis of constant cohesion. Dashed lines: flow functions estimated from the shapes of the heaps of Fig. 10 with the hypothesis of a cohesion proportional to the consolidation (upper line: fine dolomite, lower line: mixed dolomite).

*Cohesion proportional to the consolidation*—in this case, the major principal stress $\sigma_1$ is linked to the cohesion by:

$$\frac{\sigma_1}{c} = \frac{1}{\tan\delta - \mu}\left(1 + \tan\delta \frac{1 - \sin\phi}{\cos\phi}\right). \tag{21}$$

This expression has been computed using the $\phi$ values of Table 1 and the angle $\delta$ deduced from the slope $\psi$. Where $\delta = (\psi + \phi)/2$. The ratio $\sigma_1/c$ obtained leads to the two dashed lines presented on Fig. 11, the upper line for the mixed dolomite, and the lower line for the fine dolomite. Here again, the agreement with the flow function measured by the Jenike method is quite good.

The fact that we obtain in both hypotheses the same agreement with the shear cell measurement gives some confidence to the use of angle measurements for the estimation of the cohesion since this method is not highly sensitive to the model employed. The use of both approximations gives a range of uncertainty due to the method, which is quite good in the case of the dolomite powders tested whose behaviour is intermediate between the two theoretically investigated.

## 5. Concluding remarks

We discuss the feasibility of measuring the cohesion of a powder using a slope measurement of a pile formed by this powder. The theoretical study gives the shape expected in two cases: constant cohesion and cohesion proportional to consolidation for 2-dimensional heaps. It is not limitative for comparison with experimental 3-D heaps since this comparison is known to be very robust for non-cohesive powders for which the heap slope is the coefficient of friction measured in shear experiments.

For both cases (constant cohesion or cohesion proportional to consolidation), an information about the cohesion of the powder may be extracted if the friction angle $\phi$ may be measured in addition to the slope angle $\psi$. This has been checked successfully using dolomite powders of different sizes, but the issue of an independent measurement of the friction angle $\phi$ remains to be solved.

This double angle measurement issue enlightens and gives credit to the Carr's empirical indices [5], where an angle of repose and an angle of fall are measured. In return, the idea to perturb the powder heap by taps is interesting. With extra forces larger than the gravitational forces, we may reduce the cohesive length $\lambda$ enough to obtain a pile with the slope $\phi$. Preliminary experiments with the dolomite powders show that taps after the formation of the heap are not sufficient to obtain this angle. We are currently investigating experiments where vertical sinusoidal vibrations of acceleration greater than the gravity acceleration are applied during the heap formation in order to obtain heaps of slope the friction angle like non-cohesive heaps.

## References


[1] R.M. Nedderman, Statics and Kinematics of Granular Materials, Cambridge University, Cambridge, 1992.

[2] L. Bocquet, F. Restagno, E. Charlaix, European Physical Journal. E 14 (2004) 177.

[3] S. Ose, S.R. de Silva, Preliminary results from an international project on comparative characterisation of powders, Proceedings of the 3rd Israeli Conference for Conveying and Handling of Particulate Solids, the Dead Sea, Israel, 2000.

[4] ASTM Standard D 6128-97, Standard Shear Testing Method for Bulk Solids Using the Jenike Shear Cell.

[5] R.L. Carr, Chemical Engineering 72 (1965) 163.